Research Article

Journal of the Optical Society of America B

OPTICAL PHYSICS

# Bound state in the continuum in an anisotropic photonic crystal supported by a full-wave phase plate

PAVEL S. PANKIN,[1,2,†,*] DMITRII N. MAKSIMOV,[1,2,†] AND IVAN V. TIMOFEEV[1,2]

[1]Kirensky Institute of Physics, FRC KSC SB RAS, Krasnoyarsk 660036, Russia
[2]Siberian Federal University, Krasnoyarsk 660041, Russia
*Corresponding author: pavel-s-pankin@iph.krasn.ru

Received 13 December 2021; revised 31 January 2022; accepted 11 February 2022; posted 14 February 2022; published 8 March 2022

**We consider bound states in the continuum (BICs) in a 1D multilayered system of an anisotropic defect layer embedded into an anisotropic photonic crystal. We analytically demonstrate that an anisotropic defect layer embedded into anisotropic photonic crystal supports accidental BICs. These BICs can be transformed to high-Q resonances by variation of one of the system's parameters. At the same time, the BICs are remarkably robust in the sense that a true BIC can be recovered by further tuning any of the system's other parameters, leading to tunability of the resonance position.** 

https://doi.org/10.1364/JOSAB.451034

## 1. INTRODUCTION

Multilayered microcavities based on 1D photonic crystals (PhCs) have found a broad range of applications in modern photonics. The microcavities are widely used in lasers, thermal emitters, single photon sources, light emitting diodes, filters, sensors, solar cells, and absorbers [1,2]. The problem of external control of multilayered microcavity resonances addresses their spectral positions and quality factors (Q-factors). The first part of the problem is solved by adjustment of the optical thicknesses of the layers that shift the spectral position. Various functional materials have been proposed for this purpose [3–8], specifically liquid crystals [9–13]. For the second part, the control of the Q-factor can be achieved by utilizing recently emerged bound states in the continuum (BICs) [14–18].

Application of BICs allows for engineering optical modes with tunable Q-factors through controlling the energy decay rates from the localized state into the continuum of scattering channels by varying parameters of the BIC host structure. The Q-factor can reach extremely high values on approach to the BIC, being restricted only by material losses and fabrication inaccuracies. By now, several models for controlling the Q-factor in multilayered structures have been proposed theoretically [19–21] and implemented experimentally [22,23].

The system under scrutiny was proposed in our previous papers where we found that an anisotropic defect layer (ADL) embedded into an anisotropic PhC can support symmetry protected BICs due to the orthogonality between the localized state and the scattering channels [19,21]. Here, we further extend our studies by analytically and numerically demonstrating that the proposed system can also support BICs of an interference nature (accidental [24] or Friedrich–Wintgen [25] BIC mechanisms). Accidental BICs are a result of fully destructive interference of outgoing resonant modes when they leak into the scattering channels, even if the symmetry is broken. Unlike symmetry-protected BICs, accidental BICs are more robust to variation of optical and geometric parameters. It is a quite general phenomenon, reported for both 2D [26] and 3D [27–30] photonic systems.

The simplest scheme for constructing accidental BICs includes two resonance modes (or resonant pathways) and a single scattering channel. The last condition can be achieved in an anisotropic layered structure operating at different total internal reflection angles [22], in isotropic PhC operating at Brewster's angle [23], or in anisotropic PhC [19] at normal incidence. In this paper, for the first time, we derive analytical conditions for accidental BICs in anisotropic PhC and examine their robustness.

## 2. SYSTEM

The considered system is an anisotropic one-dimensional PhC with an ADL of thickness $L$ schematically pictured in Fig. 1. PhC consists of alternating isotropic and anisotropic dielectric layers arranged along the $z$ axis with period $\Lambda$. The thicknesses and permittivities of anisotropic and isotropic layers are $d$, $\epsilon_e$, $\epsilon_o$ and $\Lambda - d$, $\epsilon_o$, respectively. The optical axis of all anisotropic layers is parallel to the $x$ axis. The ADL is made of the same anisotropic material with tilted optical axis orientation determined by the unit vector

$$\boldsymbol{a} = [\cos(\phi), \sin(\phi), 0], \tag{1}$$

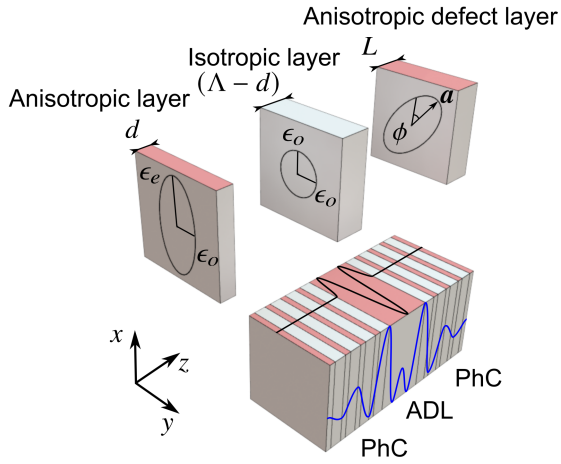


**Fig. 1.** One-dimensional anisotropic PhC structure with ADL inserted in the center of the structure. Analytic solution for the BIC mode profile: $x$-wave component Re($E_x$) (blue) and $y$-wave component Re($E_y$) (black).

where $\phi$ is the tilt angle (see Fig. 1). The corresponding dielectric tensor in the ADL is described as

$$\hat{\epsilon} = \begin{Bmatrix} \epsilon_e \cos^2(\phi) + \epsilon_o \sin^2(\phi) & \sin(2\phi)(\epsilon_e - \epsilon_o)/2 \\ \sin(2\phi)(\epsilon_e - \epsilon_o)/2 & \epsilon_e \sin^2(\phi) + \epsilon_o \cos^2(\phi) \end{Bmatrix}. \tag{2}$$

The Maxwell's equations governing propagation of a monochromatic electromagnetic wave in non-magnetic anisotropic media at normal incidence are [31]

$$\begin{Bmatrix} 0 & \nabla\times \\ -\nabla\times & 0 \end{Bmatrix} \begin{Bmatrix} \boldsymbol{E} \\ \boldsymbol{B} \end{Bmatrix} = -ik_0 \begin{Bmatrix} \hat{\epsilon}\boldsymbol{E} \\ \boldsymbol{B} \end{Bmatrix}, \tag{3}$$

where $\boldsymbol{E}$ is the electric vector, $\boldsymbol{B}$ is the magnetic vector, $k_0 = \omega/c$ is the wavenumber in vacuum, and $c$ is the speed of light.

Figure 2(a) shows the reflectance spectrum of the system surrounded by air. Although the PhC arms are always transparent to $y$-polarized waves ($y$-waves), the reflectance exhibits a peak at the $x$-polarized waves ($x$-waves) bandgap region, which is caused by periodically alternating permittivities $\epsilon_e$ and $\epsilon_o$ [32]. This dip is due to a high-quality resonant mode predicted in [19]. One can see that at $\phi = 0, \pi/2$, the resonant line collapses, indicating a symmetry protected BIC. As can be seen from the spectra in Figs. 2(b)–2(d), the increase in ADL thickness also leads to collapsing Fano features at ADL rotation angles different from $\phi = 0, \pi/2$. Thus, we conclude that the BIC persists despite the broken symmetry, i.e., the BIC occurs via the accidental [24] or Friedrich–Wintgen BIC mechanisms [25]. It is worth to point out that under given $\epsilon_o$ and $\epsilon_e$, the ADL thickness leading to the Fano feature collapse does not depend on the ADL rotation angle $\phi$. It is clearly seen from Figs. 2(b)–2(d) that the Fano feature collapse in all subplots arises for ADL thickness $L = 1$ μm despite different ADL rotation angles $\phi = \pi/8,\ \pi/4,\ 3\pi/8$. The explanation for that is provided in Section 4 based on the analytic solution for BIC condition (20).

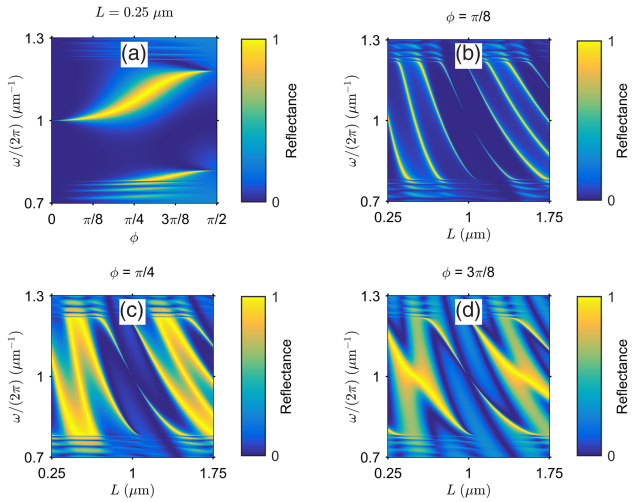


**Fig. 2.** Reflectance spectra computed by Berreman transfer matrix method for the structure containing 20 periods in each PhC arm. (a) Reflectance against the incident frequency and the ADL rotation angle $\phi$ at constant ADL thickness $L = 0.250$ μm. Collapsing Fano resonance at $\phi = 0, \pi/2$ corresponds to symmetry-protected BICs. (b)–(d) Reflectance against the incident frequency and ADL thickness $L$ at fixed rotation angles $\phi = \pi/8$ (b), $\pi/4$ (c), $3\pi/8$ (d). Collapsing resonance at $L = 1$ μm corresponds to accidental BIC. The parameters are $\epsilon_e = 4$, $\epsilon_o = 1$, $d = 0.125$ μm, $(\Lambda - d) = 0.250$ μm, and number of periods in each PhC arm is 20.

## 3. RESONANT EIGENMODE

The dispersion equation for resonant eigenfrequencies in our structure can be obtained by the wave matching method. Let us write the general solution to Maxwell's Eq. (3) in the ADL and in the PhC arms. The general solution in the ADL, $z \in [-L/2,\ L/2]$, is written as a sum of forward (+) and backward (−) propagating ordinary and extraordinary waves:

$$\boldsymbol{E} = \sum_{j=o,e} \left( \boldsymbol{E}_j^{(+)} e^{ik_j z} + \boldsymbol{E}_j^{(-)} e^{-ik_j z} \right),$$

$$\boldsymbol{B} = \sum_{j=o,e} \left( \boldsymbol{B}_j^{(+)} e^{ik_j z} + \boldsymbol{B}_j^{(-)} e^{-ik_j z} \right). \tag{4}$$

Here, $\boldsymbol{E}_j^{(\pm)}$ and $\boldsymbol{B}_j^{(\pm)}$ $(j = o, e)$ are electric and magnetic vectors of the $e$-wave and $o$-wave, respectively [33]:

$$\boldsymbol{E}_e^{(\pm)} = E_e^{(\pm)} \boldsymbol{a},\ \ \boldsymbol{B}_e^{(\pm)} = \frac{k_e}{k_0} \left[ \boldsymbol{\kappa}^{(\pm)} \times \boldsymbol{E}_e^{(\pm)} \right], \tag{5}$$

$$\boldsymbol{E}_o^{(\pm)} = E_o^{(\pm)} \left[ \boldsymbol{a} \times \boldsymbol{\kappa}^{(\pm)} \right],\ \ \boldsymbol{B}_o^{(\pm)} = \frac{k_o}{k_0} \left[ \boldsymbol{\kappa}^{(\pm)} \times \boldsymbol{E}_o^{(\pm)} \right], \tag{6}$$

where $E_e^{(\pm)}$ and $E_o^{(\pm)}$ are unknown amplitudes, $k_e = k_0\sqrt{\epsilon_e} = k_0 n_e$, $k_o = k_0\sqrt{\epsilon_o} = k_0 n_o$, and $\boldsymbol{\kappa}^{(\pm)} = [0, 0, \pm 1]$ is the unit vector along the propagation direction.

The general solution in the PhC arms for $x$-waves with field components $E_x$ and $B_y$ in the isotropic layer with the cell number $m, z \in [L/2 + m\Lambda,\ L/2 + (m+1)\Lambda - d]$, are written as

$$E_x^{(m)} = e^{iK\Lambda m}\left[A^{(+)}e^{ik_o(z-L/2-m\Lambda)} + A^{(-)}e^{-ik_o(z-L/2-m\Lambda)}\right],$$

$$B_y^{(m)} = \frac{k_o}{k_0}e^{iK\Lambda m}\left[A^{(+)}e^{ik_o(z-L/2-m\Lambda)} - A^{(-)}e^{-ik_o(z-L/2-m\Lambda)}\right], \tag{7}$$

where $K$ is the Bloch wavenumber. In the anisotropic layer with the cell number $m$, $z \in [L/2+(m+1)\Lambda - d,\ L/2+(m+1)\Lambda]$, we have

$$E_x^{(m)} = e^{iK\Lambda m}\left[B^{(+)}e^{ik_e(z-L/2-(m+1)\Lambda+d)} + B^{(-)}e^{-ik_e(z-L/2-(m+1)\Lambda+d)}\right],$$

$$B_y^{(m)} = \frac{k_e}{k_0}e^{iK\Lambda m}\left[B^{(+)}e^{ik_e(z-L/2-(m+1)\Lambda+d)} - B^{(-)}e^{-ik_e(z-L/2-(m+1)\Lambda+d)}\right]. \tag{8}$$

The outgoing wave is $y$ polarized since it is not affected by the PhC arm:

$$E_y = -C^{(+)}e^{ik_o(z-L/2)},$$

$$B_x = \frac{k_o}{k_0}C^{(+)}e^{ik_o(z-L/2)}. \tag{9}$$

By applying the continuity condition for the tangential field components (7) and (8) between the PhC arm layers, one can obtain the following equations that govern the propagation of the $x$-waves in the PhC arm:

$$\begin{cases} A^{(+)}\left[e^{ik_o(\Lambda-d)} - e^{iK\Lambda}e^{-ik_e d}\right] - A^{(-)}r_{oe}\left[e^{-ik_o(\Lambda-d)} - e^{iK\Lambda}e^{-ik_e d}\right] = 0, \\ -A^{(+)}r_{oe}\left[e^{ik_o(\Lambda-d)} - e^{iK\Lambda}e^{ik_e d}\right] + A^{(-)}\left[e^{-ik_o(\Lambda-d)} - e^{iK\Lambda}e^{ik_e d}\right] = 0, \end{cases} \tag{10}$$

where $r_{oe} = (k_o - k_e)/(k_o + k_e)$ is the Fresnel coefficient.

The mirror symmetry of the system is exploited to write the solution in the left PhC arm. In the antisymmetric case, we have

$$\boldsymbol{E}(z) = -\boldsymbol{E}(-z), \tag{11}$$

while in the symmetric case, the condition is

$$\boldsymbol{E}(z) = \boldsymbol{E}(-z). \tag{12}$$

By matching Eqs. (4), (7), and (9) on the interface between the ADL and the right PhC arm and using Eqs. (10), (11), and (12), we can obtain the final dispersion equation

$$\frac{\xi e^{ik_o(\Lambda-d)} - r_{oe}e^{-ik_o(\Lambda-d)}}{\xi e^{-ik_e d} - r_{oe}e^{-ik_e d}} - \frac{e^{-ik_o(\Lambda-d)} - \xi r_{oe}e^{ik_o(\Lambda-d)}}{e^{ik_e d} - \xi r_{oe}e^{ik_e d}} = 0, \tag{13}$$

where

$$\xi = -e^{ik_o L}\sin^2(\phi) + \frac{r_{oe} - e^{ik_e L}}{1 - r_{oe}e^{ik_e L}}\cos^2(\phi) \tag{14}$$

for the antisymmetric case, and

$$\xi = e^{ik_o L}\sin^2(\phi) + \frac{r_{oe} + e^{ik_e L}}{1 + r_{oe}e^{ik_e L}}\cos^2(\phi), \tag{15}$$

for the symmetric case. Equations (13)–(15) are solved for the complex eigenfrequency

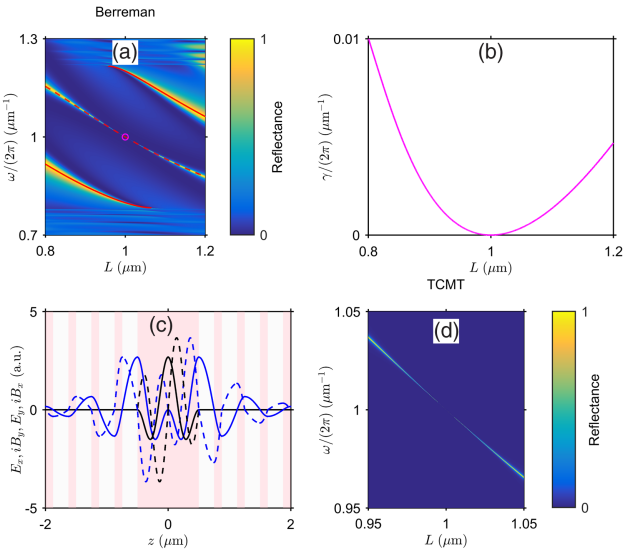


**Fig. 3.** (a) Zoomed-in reflectance spectrum from Fig. 2(c). Solid red lines show the real part of solution to Eqs. (13) and (14) in the antisymmetric case. The dashed line demonstrates the symmetric solution obtained from Eqs. (13) and (15). The magenta circle shows the position of the BIC from Eq. (20). (b) Imaginary part of solution (13), (15). (c) BIC field profile (21)–(23). All parameters are identical to those in the Fig. 2(c) caption. The normalization condition is used (24) to yield $A = \sqrt{2\pi/7}$. (d) Reflectance spectrum obtained by temporal coupled-mode theory (TCMT), Eq. (26).

$$\omega_r = \tilde{\omega} - i\gamma. \tag{16}$$

The real part of the eigenfrequency $\tilde{\omega}$ determines the position of the resonance. The position of the resonance is shown in Fig. 3(a), superposed with the reflectance spectrum. The imaginary part of the eigenfrequency that determines the FWHM of the resonance $\Delta\omega = 2\gamma$ predicts a collapsing Fano feature at the same point as found from the numerical reflectance spectrum Fig. 3(b). Let us show that the point of collapse corresponds to a BIC.

## 4. BOUND STATE IN THE CONTINUUM

To find the solution for an accidental BIC in the symmetric case, we match Eqs. (4), (7), and (9) on the boundary between the ADL and the PhC arms using (10) and (12) together with the condition on destructive interference between ordinary and extraordinary waves projected on the $y$ axis:

$$E_y(L/2) = 0,\ B_x(L/2) = 0. \tag{17}$$

The solution for the BIC takes the following form:

$$n_o \tan(k_o L/2) - n_e \tan(k_e L/2) = 0. \tag{18}$$

Equation (18) transforms to identity when two conditions are simultaneously fulfilled:

$$k_o L/2 = m_1\pi,\ k_e L/2 = m_2\pi,\ m_{1,2} \in \mathbb{N}. \tag{19}$$

In the simplest case of $m_2 = m_1 + 1$, we have a full-wave phase plate condition:

$$(k_e - k_o)L = 2\pi. \tag{20}$$

The solution (20) shown in Fig. 3(a) by a magenta circle corresponds to the collapse of the Fano feature. The full-wave phase plate preserves the linear polarization of the incident wave independent of orientation of the optical axis. Therefore, the tilt angle is absent from both the final solution for the BIC, Eq. (18), and the reflectance spectra in Fig. 2.

The BIC field profile inside the ADL is

$$\begin{cases} E_x = 2A(\cos(k_e z)\cot(\phi)\cos(\phi) - \cos(k_o z)\sin(\phi)), \\ B_y = 2iA(n_e \sin(k_e z)\cot(\phi)\cos(\phi) - n_o \sin(k_o z)\sin(\phi)), \\ E_y = 2A(\cos(k_e z) + \cos(k_o z))\cos(\phi), \\ B_x = -2iA(n_e \sin(k_e z) + n_o \sin(k_o z))\cos(\phi). \end{cases} \tag{21}$$

Inside the PhC arms, in the isotropic layer with the cell number $m$, $z \in [L/2 + m\Lambda,\ L/2 + (m+1)\Lambda - d]$, we have

$$\begin{cases} E_x^{(m)} = \frac{2A}{\sin(\phi)}(-q)^m \cos(k_o(z - L/2 - m\Lambda)), \\ B_y^{(m)} = \frac{2iA}{\sin(\phi)}(-q)^m n_o \sin(k_o(z - L/2 - m\Lambda)), \\ E_y = 0, \\ B_x = 0. \end{cases} \tag{22}$$

Finally, inside the PhC arms, in the anisotropic layer with the cell number $m$, $z \in [L/2 + (m+1)\Lambda - d,\ L/2 + (m+1)\Lambda]$, we have

$$\begin{cases} E_x^{(m)} = \frac{2A}{\sin(\phi)}(-q)^{m+1} \sin(k_e(z - L/2 - (m+1)\Lambda + d)), \\ B_y^{(m)} = -\frac{2iA}{\sin(\phi)}(-q)^{m+1} n_e \cos(k_e(z - L/2 - (m+1)\Lambda + d)), \\ E_y = 0, \\ B_x = 0. \end{cases} \tag{23}$$

Here, $q = n_o/n_e$, and the amplitude $A$ has to be defined from a proper normalization condition, for example, by equating the total energy of BIC $\mathcal{E}$ to unity:

$$\mathcal{E} = \frac{1}{8\pi}\int_{-\infty}^{+\infty} \mathrm{d}z \left[E^\dagger \hat{\epsilon}(z) E + B^\dagger B\right] = 1, \tag{24}$$

where

$$\boldsymbol{E} = \begin{Bmatrix} E_x \\ E_y \end{Bmatrix}, \quad \boldsymbol{B} = \begin{Bmatrix} B_x \\ B_y \end{Bmatrix}. \tag{25}$$

The BIC field profile is shown in Figs. 1 and 3(c).

## 5. TCMT AND ROBUSTNESS OF THE BIC

The general expression for the reflection/transmission amplitudes was obtained in [19] based on temporal coupled mode theory (TCMT) [34] as

$$\rho = \frac{i\gamma}{(\tilde{\omega} - \omega) + i\gamma}, \quad \tau = 1 - \rho, \tag{26}$$

where $\tilde{\omega}$ and $\gamma$ are real and imaginary parts of the resonant eigenfrequency (16), and $\omega$ is the incident frequency. The single resonance solution (26) coincides with the numerical data to good accuracy [see Fig. 3(d)].

According to Eq. (26), the reflectance depends only on two parameters, $\gamma$ and $\tilde{\omega}$. The radiative decay rate $\gamma$ can be controlled by detuning one of the system's parameters from the BIC point (see Fig. 2). Technically, both $\tilde{\omega}$ and $\gamma$ can be found from solving Eqs. (13) and (15). In Fig. 4, we show the position of the BIC as a function any pair of two parameters $L$, $n_e$, $n_o$. One can see that the positions of the BIC form continuous lines in all the considered cases. In other words, after variation of a single parameter, any other parameter can be tuned to recover a BIC, making it robust with respect to parameter variation.

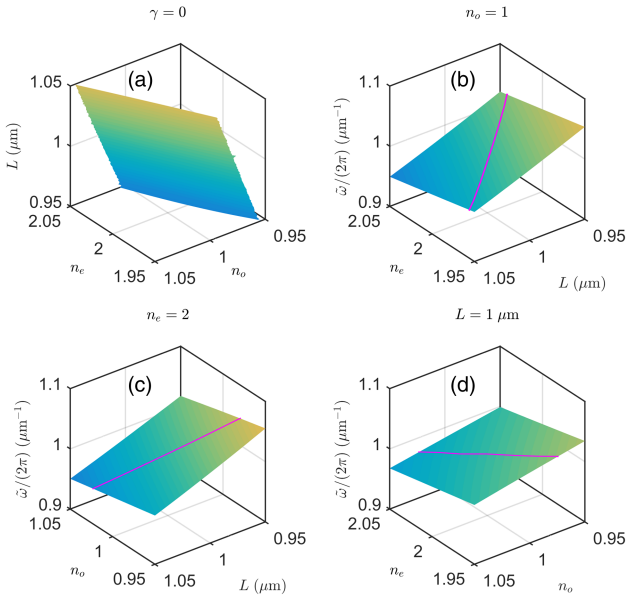


**Fig. 4.** (a) Solution to Eqs. (13) and (15) with $\gamma = 0$ (BIC). (b)–(d) Real part of the solution to Eqs. (13) and (15) in the symmetric case. Magenta lines show the positions of the BIC ($\gamma = 0$). Parameters are the same as in the Fig. 2(c) caption.

## 6. CONCLUSION

In this paper, we considered BICs in a 1D multilayered system of an ADL embedded into an anisotropic PhC. We analytically demonstrated that the PhC-embedded full-wave phase plate ADL supports accidental BICs. These BICs can be transformed to high-Q resonances by variation of one of the system's parameters, allowing for control of the resonant width. At the same time, the BICs are remarkably robust in the sense that a true BIC can be recovered by further tuning any of the system's other parameters, leading to tunability of the resonance position. The demonstrated effect will lead to robustness of the BIC supporting setup with respect to fabrication tolerance, paving the way for implementing microcavities with tunable Q-factors.

**Funding.** Council on Grants of the President of the Russian Federation (MK-4012.2021.1.2).

**Acknowledgment.** The authors are grateful to V.A. Stepanenko (Siberian Federal University) for helpful discussions. P. S. Pankin is grateful for the support of the President of the Russian Federation.

**Disclosures.** The authors declare no conflicts of interest.

**Data availability.** The data that support the findings of this study are available within the paper.

[†]These authors contributed equally to this work.

## REFERENCES


1. J. D. Joannopoulos, S. G. Johnson, J. N. Winn, and R. D. Meade, *Photonic Crystals: Molding the Flow of Light*, 2nd ed. (Princeton University, 2008).
2. A. V. Kavokin, J. J. Baumberg, G. Malpuech, and F. P. Laussy, *Microcavities* (Oxford University, 2017), Vol. **21**.
3. Y.-H. Chang, Y.-Y. Jhu, and C.-J. Wu, "Temperature dependence of defect mode in a defective photonic crystal," Opt. Commun. **285**, 1501–1504 (2012).
4. J. Yoon, W. Lee, J.-M. Caruge, M. Bawendi, E. L. Thomas, S. Kooi, and P. N. Prasad, "Defect-mode mirrorless lasing in dye-doped organic/inorganic hybrid one-dimensional photonic crystal," Appl. Phys. Lett. **88**, 091102 (2006).
5. A. H. Aly, F. A. Sayed, and H. A. Elsayed, "Defect mode tunability based on the electro-optical characteristics of the one-dimensional graphene photonic crystals," Appl. Opt. **59**, 4796 (2020).
6. A. H. Aly and H. A. ElSayed, "Tunability of defective one-dimensional photonic crystals based on Faraday effect," J. Mod. Opt. **64**, 871–877 (2017).
7. F. Segovia-Chaves and H. A. Elsayed, "Pressure-based defect mode tunability in a one-dimensional photonic crystal composed of $SiO_2$ and Si," Optik **247**, 167802 (2021).
8. T. Goto, A. V. Dorofeenko, A. M. Merzlikin, A. V. Baryshev, A. P. Vinogradov, M. Inoue, A. A. Lisyansky, and A. B. Granovsky, "Optical Tamm states in one-dimensional magnetophotonic structures," Phys. Rev. Lett. **101**, 14–16 (2008).
9. S. Y. Vetrov and A. V. Shabanov, "Localized electromagnetic modes and the transmission spectrum of a one-dimensional photonic crystal with lattice defects," J. Exp. Theor. Phys. **93**, 977–984 (2001).
10. R. Ozaki, T. Matsui, M. Ozaki, and K. Yoshino, "Electrically color-tunable defect mode lasing in one-dimensional photonic-band-gap system containing liquid crystal," Appl. Phys. Lett. **82**, 3593–3595 (2003).
11. V. G. Arkhipkin, V. A. Gunyakov, S. A. Myslivets, V. P. Gerasimov, V. Y. Zyryanov, S. Y. Vetrov, and V. F. Shabanov, "One-dimensional photonic crystals with a planar oriented nematic layer: temperature and angular dependence of the spectra of defect modes," J. Exp. Theor. Phys. **106**, 388–398 (2008).
12. V. G. Arkhipkin, V. A. Gunyakov, S. A. Myslivets, V. Y. Zyryanov, V. F. Shabanov, and W. Lee, "Electro- and magneto-optical switching of defect modes in one- dimensional photonic crystals," J. Exp. Theor. Phys. **112**, 577–587 (2011).
13. P. S. Pankin, V. S. Sutormin, V. A. Gunyakov, F. V. Zelenov, I. A. Tambasov, A. N. Masyugin, M. N. Volochaev, F. A. Baron, K. P. Chen, V. Y. Zyryanov, S. Y. Vetrov, and I. V. Timofeev, "Experimental implementation of tunable hybrid Tamm-microcavity modes," Appl. Phys. Lett. **119**, 161107 (2021).
14. C. W. Hsu, B. Zhen, A. D. Stone, J. D. Joannopoulos, and M. Soljačić, "Bound states in the continuum," Nat. Rev. Mater. **1**, 16048 (2016).
15. K. Koshelev, A. Bogdanov, and Y. Kivshar, "Meta-optics and bound states in the continuum," Sci. Bull. **64**, 836–842 (2019).
16. S. I. Azzam and A. V. Kildishev, "Photonic bound states in the continuum: from basics to applications," Adv. Opt. Mater. **9**, 2001469 (2021).
17. A. F. Sadreev, "Interference traps waves in open system: bound states in the continuum," Rep. Prog. Phys. **84**, 55901 (2021).
18. S. Joseph, S. Pandey, S. Sarkar, and J. Joseph, "Bound states in the continuum in resonant nanostructures: an overview of engineered materials for tailored applications," Nanophotonics **10**, 4175–4207 (2021).
19. I. V. Timofeev, D. N. Maksimov, and A. F. Sadreev, "Optical defect mode with tunable Q factor in a one-dimensional anisotropic photonic crystal," Phys. Rev. B **97**, 24306 (2018).
20. D. O. Ignatyeva and V. I. Belotelov, "Bound states in the continuum enable modulation of light intensity in the Faraday configuration," Opt. Lett. **45**, 6422–6425 (2020).
21. P. S. Pankin, D. N. Maksimov, K.-P. Chen, and I. V. Timofeev, "Fano feature induced by a bound state in the continuum via resonant state expansion," Sci. Rep. **10**, 13691 (2020).
22. J. Gomis-Bresco, D. Artigas, and L. Torner, "Anisotropy-induced photonic bound states in the continuum," Nat. Photonics **11**, 232–236 (2017).
23. P. S. Pankin, B.-R. Wu, J.-H. Yang, K.-P. Chen, I. V. Timofeev, and A. F. Sadreev, "One-dimensional photonic bound states in the continuum," Commun. Phys. **3**, 91 (2020).
24. C. W. Hsu, B. Zhen, J. Lee, S.-L. Chua, S. G. Johnson, J. D. Joannopoulos, and M. Soljačić, "Observation of trapped light within the radiation continuum," Nature **499**, 188–191 (2013).
25. H. Friedrich and D. Wintgen, "Interfering resonances and bound states in the continuum," Phys. Rev. A **32**, 3231–3242 (1985).
26. A. I. Ovcharenko, C. Blanchard, J.-P. Hugonin, and C. Sauvan, "Bound states in the continuum in symmetric and asymmetric photonic crystal slabs," Phys. Rev. B **101**, 155303 (2020).
27. E. A. Bezus, D. A. Bykov, and L. L. Doskolovich, "Bound states in the continuum and high-Q resonances supported by a dielectric ridge on a slab waveguide," Photon. Res. **6**, 1084–1093 (2018).
28. T. G. Nguyen, G. Ren, S. Schoenhardt, M. Knoerzer, A. Boes, and A. Mitchell, "Ridge resonance in silicon photonics harnessing bound states in the continuum," Laser Photon. Rev. **13**, 1900035 (2019).
29. D. A. Bykov, E. A. Bezus, and L. L. Doskolovich, "Coupled-wave formalism for bound states in the continuum in guided-mode resonant gratings," Phys. Rev. A **99**, 063805 (2019).
30. M. V. Rybin, K. L. Koshelev, Z. F. Sadrieva, K. B. Samusev, A. A. Bogdanov, M. F. Limonov, and Y. S. Kivshar, "High-Q supercavity modes in subwavelength dielectric resonators," Phys. Rev. Lett. **119**, 243901 (2017).
31. R. Feynman, R. Leighton, and M. Sands, *The Feynman Lectures on Physics*, The New Millennium ed. Mainly Electromagnetism and Matter (2015), Vol. **II**.
32. S. M. Rytov, "Electromagnetic properties of a finely stratified medium," Sov. Phys. JETP **2**, 466–475 (1956).
33. F. V. Ignatovich and V. K. Ignatovich, "Optics of anisotropic media," Uspekhi Fiz. Nauk **182**, 759 (2012).
34. S. Fan, W. Suh, and J. D. Joannopoulos, "Temporal coupled-mode theory for the Fano resonance in optical resonators," J. Opt. Soc. Am. A **20**, 569–572 (2003).